Locking Range Derivations for Injection-Locked Class-E Oscillator Applying Phase Reduction Theory

Tomoharu Nagashima, *Student Member, IEEE*, Xiuqin Wei, *Member, IEEE*, Hisa-Aki Tanaka, *Member, IEEE*, and Hiroo Sekiya, *Senior Member, IEEE*

Abstract—This paper presents a numerical locking-range prediction for the injection-locked class-E oscillator using the phase reduction theory (PRT). By applying this method to the injection-locked class-E oscillator designs, which is in the field of electrical engineering, the locking ranges of the oscillator on any injection-signal waveform can be efficiently obtained. The locking ranges obtained from the proposed method quantitatively agreed with those obtained from the simulations and circuit experiments, showing the validity and effectiveness of the locking-range derivation method based on PRT.

Index Terms—Injection-locked class-E oscillator, locking range, phase reduction theory.

I. INTRODUCTION

IN RECENT years, resonant class-D [1], class-E [2]–[14], and class-DE [15] power oscillators have been widely used in various applications. These resonant power oscillators are oscillated by the feedback voltage transformed from the output voltage. Class-E and class-DE oscillators can achieve high power-conversion efficiencies at high frequencies because of the class-E zero-voltage switching and zero-derivative switching (ZVS/ZDS) operations. Because of their high operational efficiency, these oscillators have many applications such as electric ballasts [6], [7], dc-dc converters [8], [9], and transmitters for wireless power transfer [10], [11], and wireless communication [12]. In such applications, a limitation of the oscillator is that the free-running frequency usually has a small error from the specified frequency owing to component tolerances. Therefore, accurately specified frequency operations are required for practical usage that considers the radio law and phase noise. The injection locking technique [13], [14], [16]–[33] is one solution for this problem.

In the injection-locked class-E oscillator [13], [14], the injection circuit is added to the class-E free-running oscillator for oscillation frequency stabilization. When the feedback voltage

of the free-running class-E oscillator is synchronized with the small injection signal, the frequency of the class-E oscillator can be fixed at the injection signal frequency. The locking range prediction for the injection-locked resonant power oscillator is very important and useful for oscillator design [18], [19]. This is because the required injection power for the synchronization can be estimated in the design process.

Analytical expressions of the locking ranges have been previously reported [13] on the basis of Adler's equation [16]–[22]. From these analytical expressions, the locking ranges of injection-locked class-E oscillator can be approximately estimated. This analysis is, however, only valid for the case in which the injection signal is a sinusoidal waveform. For the implementation point of view, it is useful to predict the locking ranges on various injection-signal waveforms. In previous research [14], the locking ranges for the injection-locked class-E oscillator with various injection signal waveforms were numerically obtained. It was also shown that the locking ranges depend on the injection-signal waveform [14]; however, the numerical derivations of locking ranges in this study require high computation cost.

The phase reduction theory (PRT) [24]–[31] is an analysis method developed in the field of physics used for investigating the synchronization phenomena. By expressing the oscillator dynamics as functions of phase variables, the synchronization range can be easily and accurately obtained. The phase sensitivity function (PSF) represents a phase gradient on the limit cycle of the oscillator, which is the most important function used for investigating the synchronization ranges in PRT. The locking range can be obtained from the convolution integral of the PSF and the function of the injection signal. In previous research [29]–[31], PRT has been applied to the weakly coupled oscillators, such as Sturart-Landau and van der Pol oscillators, which shows the utility of PRT. Nevertheless, PRT has never been fully utilized in the research field of power electronics. In this sense, it is important to show that PRT can be applied to the design of resonant power oscillators as an application example.

The objective of this study is to present the feasibility of locking range predictions of the resonant power oscillator by PRT. To our knowledge, our study here is the first paper to show a systematic design process with respect to the locking ranges of the resonant oscillator, which can be applied to other injection-locked resonant-power-oscillator designs. It is shown that PRT is quite useful for obtaining the locking ranges of injection-locked class-E oscillators. By applying PRT, it is possible to obtain the locking ranges on any injection-signal waveform at a low computation cost. By conducting simulations and circuit experiments, it was confirmed that the locking ranges predicted by the proposed method quantitatively agree with those obtained from the simulations and circuit experiments, thereby

Fig. 1. Circuit descriptions. (a) Injection-locked class-E oscillator. (b) Equivalent circuit.

Fig. 2. Nominal waveforms of free-running class-E oscillator.

demonstrating the validity and effectiveness of the proposed locking-range-derivation method based on PRT.

II. INJECTION-LOCKED CLASS-E OSCILLATOR

Fig. 1(a) shows the circuit topology of the injection-locked class-E oscillator [13], [14]. This circuit consists of the class-E free-running oscillator [2]–[5] and injection circuit. The class-E free-running oscillator has dc-supply voltage V_{DD}, dc-feed inductance L_C, MOSFET as a switching device S, shunt capacitance C_S, series resonant circuit $L_0 - C_0 - R$, voltage-dividing capacitances C_1 and C_2, feedback inductance L_f for phase shifting, and resistances R_{d1} and R_{d2} for supplying the bias voltage across the gate-to-source of the MOSFET, which are sufficiently large to neglect the current through them.

Fig. 2 shows example waveforms of the free-running class-E oscillator, particularly for $v_{inj} = 0$ in Fig. 1(a). Generally, the resonant circuit $L_0 - C_0 - R$ in the oscillator has a high quality factor Q. Therefore, the current through the resonant circuit i is regarded as a pure sinusoidal current. The feedback voltage v_f, which is obtained from the output voltage, controls the MOSFET. During $v_f \geq V_{th}$, the MOSFET is in the "on" state, as shown in Fig. 2, where V_{th} is the gate threshold voltage. On the contrary, in the case of $v_f < V_{th}$, the MOSFET is in the "off" state. During the switch to the off state, the current through the shunt capacitance C_S produces a pulse-like shape of voltage across the switch, as shown in Fig. 2. The switching losses are reduced to zero by the operating requirements of zero voltage and zero derivative voltage at the turn-on instant, which are known as class-E ZVS/ZDS conditions [2]–[15], [34] and are expressed as

$$v_S(2\pi) = 0 \text{ and } \left.\frac{dv_S}{d\theta}\right|_{\theta=2\pi} = 0. \tag{1}$$

The power dissipations caused in the feedback network are kept small because the current i_f through the feedback network is much smaller than the output current i.

Usually, the free-running frequency f_{free} has an error from the specified frequency. One of the techniques used to solve this problem is injection locking [13], [14], [16]–[33]. Because the injection-signal power is low, it is possible to obtain the injection-locked oscillator by just adding the injection signal to
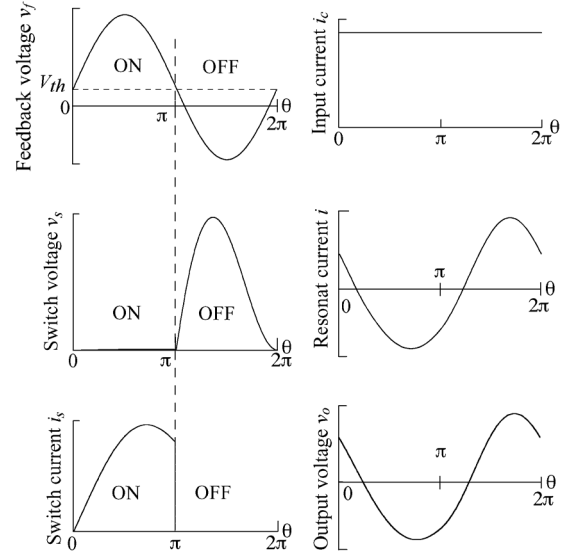
the original free-running oscillator. Therefore, the circuit design is simple even when the injection-locking technique is applied. For the injection-locked class-E oscillator used in previous studies [13], [14], a small voltage is injected into the MOSFET gate terminal, as shown in Fig. 1(a). If the feedback voltage of the class-E free-running oscillator is synchronized with the injection signal v_{inj}, the oscillation frequency is locked with the injection-signal frequency f_{inj}, which means the frequency of the output voltage is fixed with f_{inj}. It is easy to achieve synchronization as the injection-signal power increases. However, high power injection affects the waveforms of the feedback voltage and switch-on duty ratio, which yields the design complexity. It is necessary to conduct the total design of the free-running oscillator and injection circuits for large perturbation. Additionally, low injection-signal power is good from a power-added efficiency perspective.

III. PHASE REDUCTION THEORY FOR INJECTION-LOCKED OSCILLATOR

PRT [24]–[31] is an analytical method developed in the field of physics for investigating the synchronization phenomena. By expressing the oscillator dynamics as functions of phase variables, the synchronization range can be obtained easily and accurately.

A. Phase Function

It is considered that a non-perturbed dynamical system can be expressed as

$$\frac{d\boldsymbol{x}(\theta)}{d\theta} = \boldsymbol{F}(\boldsymbol{x}(\theta)), \tag{2}$$

where $\theta = \omega t = 2\pi f_{free} t \in \boldsymbol{R}$ and $\boldsymbol{x} \in \boldsymbol{R}^n$ denote the angular time with free-running frequency and the state-variation vector, respectively. In this paper, for simplicity,

$$\boldsymbol{F} : \boldsymbol{R} \times \boldsymbol{R}^n \to \boldsymbol{R}^n \ (\boldsymbol{x}(\theta)) \to \boldsymbol{F}(\boldsymbol{x}(\theta)) \tag{3}$$

is periodic in θ with period 2π as follows:

$$\boldsymbol{F}(\boldsymbol{x}(\theta + 2\pi)) = \boldsymbol{F}(\boldsymbol{x}(\theta)). \tag{4}$$

It is assumed that (2) has a solution $\boldsymbol{x}(\theta) = \boldsymbol{\varphi}(\theta)$, and that this solution has a limit cycle in the phase space, as shown in
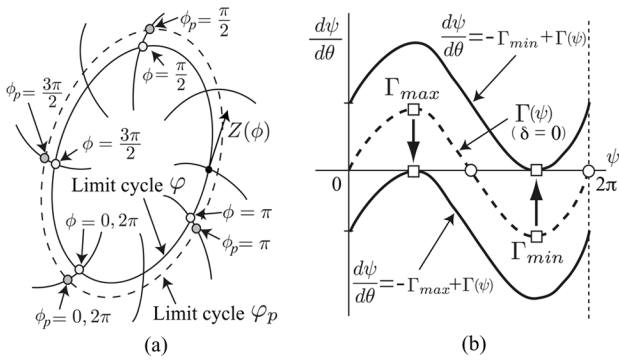
Fig. 3. Example of oscillator dynamics. (a) Limit cycle. (b) $d\psi/dt$ versus ψ.

Fig. 3(a). For the dynamical system, a phase variable is defined as

$$\phi(\boldsymbol{\varphi}) = \theta, \tag{5}$$

where ϕ has 2π-periodicity. The derivative of ϕ is obtained as

$$\begin{aligned}
\frac{d\phi}{d\theta} &= \frac{\partial\phi}{\partial\boldsymbol{x}} \cdot \frac{d\boldsymbol{\varphi}}{d\theta} \\
&= \frac{\partial\phi}{\partial\boldsymbol{x}} \cdot \boldsymbol{F}(\boldsymbol{x}(\theta)) \\
&= 1.
\end{aligned} \tag{6}$$

The perturbed dynamical system of (2) is expressed as

$$\frac{d\boldsymbol{x}(\theta)}{d\theta} = \boldsymbol{F}(\boldsymbol{x}(\theta)) + \boldsymbol{G}(\Theta), \tag{7}$$

where $\boldsymbol{G}(\Theta)$ represents the weak perturbation, which expresses the injection signal in this paper, and $\Theta = \Omega t$ is the angular time of perturbation with the angular frequency $\Omega = 2\pi f_{inj}$. It is also assumed that (7) has a solution $\boldsymbol{x}(\theta) = \boldsymbol{\varphi}_p(\theta)$. The perturbation drives the trajectory away from the limit cycle $\boldsymbol{\varphi}$. However, the trajectory $\boldsymbol{\varphi}_p$ only slightly deviates from the original trajectory $\boldsymbol{\varphi}$ because the injection signal is small if the limit cycle $\boldsymbol{\varphi}_p$ is stable. Therefore, we can define the phase ϕ_p on $\boldsymbol{\varphi}_p$ in the neighborhood of $\boldsymbol{\varphi}$, as shown in Fig. 3(a).

From (6) and (7), the phase dynamics of the perturbed dynamical system can be expressed as

$$\begin{aligned}
\frac{d\phi_p}{d\theta} &= \left.\frac{\partial\phi_p}{\partial\boldsymbol{x}}\right|_{\boldsymbol{x}=\boldsymbol{\varphi}_p(\phi_p)} \cdot \frac{d\boldsymbol{\varphi}_p}{d\theta} \\
&= \left.\frac{\partial\phi_p}{\partial\boldsymbol{x}}\right|_{\boldsymbol{x}=\boldsymbol{\varphi}_p(\phi_p)} \cdot (\boldsymbol{F}(\boldsymbol{x}(\theta)) + \boldsymbol{G}(\Theta)) \\
&= 1 + \left.\frac{\partial\phi_p}{\partial\boldsymbol{x}}\right|_{\boldsymbol{x}=\boldsymbol{\varphi}_p(\phi_p)} \cdot \boldsymbol{G}(\Theta).
\end{aligned} \tag{8}$$

When the perturbation is small, the deviation of $\boldsymbol{\varphi}_p$ from the original trajectory $\boldsymbol{\varphi}$ is also small. Therefore, $\partial\phi_p/\partial\boldsymbol{x}$, which is included in the right-hand side of (8), can be approximated as

$$\left.\frac{\partial\phi_p}{\partial\boldsymbol{x}}\right|_{\boldsymbol{x}=\boldsymbol{\varphi}_p(\phi_p)} \approx \left.\frac{\partial\phi}{\partial\boldsymbol{x}}\right|_{\boldsymbol{x}=\boldsymbol{\varphi}(\phi)} = \boldsymbol{Z}(\phi). \tag{9}$$

$\boldsymbol{Z}(\phi)$ is known as the phase sensitivity function (PSF). By substituting (9) into (8), we can obtain the phase function of the perturbed dynamical system as

$$\frac{d\phi_p}{d\theta} \approx 1 + \boldsymbol{Z}(\phi) \cdot \boldsymbol{G}(\Theta). \tag{10}$$

B. Time Averaging for Simplification

The phase difference between the perturbed limit cycle and the external force is

$$\psi = \phi_p - \Theta. \tag{11}$$

By eliminating ϕ_p from (10) and (11), we can obtain

$$\begin{aligned}
\frac{d\psi}{d\theta} &\approx 1 - \frac{d\Theta}{d\theta} + \boldsymbol{Z}(\psi + \Theta) \cdot \boldsymbol{G}(\Theta) \\
&= 1 - \frac{\Omega}{\omega} + \boldsymbol{Z}(\psi + \Theta) \cdot \boldsymbol{G}(\Theta).
\end{aligned} \tag{12}$$

Because $\Omega/\omega \approx 1$ and $\boldsymbol{G}(\Theta) \ll 1$, the variation of ψ is much slower than that of Θ. Therefore, ψ is regarded as constant during one period of the dynamical system and (12) can be simplified by averaging Θ as follows:

$$\begin{aligned}
\frac{d\psi}{d\theta} &= 1 - \frac{\Omega}{\omega} + \frac{1}{2\pi}\int_0^{2\pi} \boldsymbol{Z}(\psi + \Theta) \cdot \boldsymbol{G}(\Theta)d\Theta, \\
&= 1 - \frac{\Omega}{\omega} + \Gamma(\psi).
\end{aligned} \tag{13}$$

C. Locking Range

When $d\psi/d\theta = 0$, the original oscillator is synchronized with the weak forcing signal. Fig. 3(b) shows $d\psi/d\theta$ as a function of ψ. If there is at least one solution of $d\psi/d\theta = 0$ for ψ, the phase difference is locked in the steady state. $\Gamma(\psi)$ is a periodic function of ψ because $\boldsymbol{Z}$ and $\boldsymbol{G}$ are the 2π-periodicity functions. As shown in Fig. 3(b), $d\psi/d\theta$ has at least one solution for ψ if the $1 - \Omega/\omega$ is in the range of

$$-\Gamma_{max} \leq 1 - \frac{\Omega}{\omega} \leq -\Gamma_{min}, \tag{14}$$

where Γ_{min} and Γ_{max} are the minimum and maximum values of $\Gamma(\psi)$. From (14), the locking range is obtained as

$$\Gamma_{min} + 1 \leq \frac{\Omega}{\omega} \leq \Gamma_{max} + 1. \tag{15}$$

$\Gamma(\psi)$ can be obtained by the convolution integral of the PSF and forcing signal as given in (13). Therefore, the locking ranges of the injection-locked oscillator can be derived regardless of $\boldsymbol{G}$, particularly injection-signal waveforms, after the PSF is obtained.

IV. DESIGN OF INJECTION-LOCKED CLASS-E OSCILLATOR

A. Assumptions

For both the free-running class-E oscillator design and the locking-range derivations, it is necessary to formulate the circuit equations of the injection-locked class-E oscillator, which corresponds to (7). The circuit equations are based on the following assumptions.
  a) The MOSFET is used as a switching device S, which has zero switching times, infinite off resistance, and on resistance r_S.
  b) The MOSFET has an equivalent series capacitance and equivalent series resistance (ESR) between the gate and the source of the MOSFET, which are C_g and r_g, respectively.
  c) IRF530 MOSFET is used as a switching device S. Table I gives the IRF530 MOSFET parameters. In this table, V_{th}, r_S, and V_{fFET} were obtained from the FET manual,

Threshold voltage V_{th}	3 V
Switch on resistance r_S	0.16 Ω
Equivalent series capacitance C_g	1.78 nF
Equivalent series resistance r_g	2.17 Ω
Maximum gate-source voltage V_{fFET}	20 V

where V_{fFET} is the permissible maximum gate-source voltage. C_g and r_g were measured by HP 16047A at 1MHz.

d) All of the inductances L_C, L_0, and L_f have an ESR r_{L_C}, L_{L_0}, and r_{L_f}, respectively.

e) The shunt capacitance C_S includes the MOSFET drain-to-source parasitic capacitances.

f) All of the passive elements including switch-on resistance, MOSFET parasitic capacitances, and ESRs of inductances work as linear elements.

g) The MOSFET turns on at $\theta = 0$ and turns off at $\theta = \pi$ in the free-running operation.

From above assumptions, we have an equivalent circuit of the injection-locked class-E oscillator, as shown in Fig. 1(b).

B. Circuit Equations

From the equivalent circuit in Fig. 1(b), the circuit equations are expressed as the equation at the bottom of the page.

In (16), R_S is the equivalent resistance of the switch. According to the assumption a) and f), R_S is expressed as

$$R_S = \begin{cases} r_S & \text{for } (V_{th} - v_f) \le 0 \\ \infty & \text{for } (V_{th} - v_f) > 0 \end{cases} \qquad (17)$$

Now, $\boldsymbol{x} \in \boldsymbol{R}^9$ and $\boldsymbol{G} \in \boldsymbol{R}^9$ are defined as

$$\boldsymbol{x}(\theta) = \frac{1}{V_{DD}} [Ri_C(\theta), v_S(\theta), v(\theta), Ri(\theta), v_1(\theta), v_2(\theta),$$
$$r_g i_f(\theta), v_g(\theta), v_{C_{inj}}(\theta)]^T \quad (18)$$

and

$$\boldsymbol{G}(\Theta) = \frac{v_{inj}}{V_{DD}}[0, 0, 0, 0, 0, 0, g_1, g_2, g_3]^T, \qquad (19)$$

where

$$g_1 = -\frac{r_g}{\omega L_f R_{inj}\left(\frac{1}{r_g} + \frac{1}{R_{d1}} + \frac{1}{R_{d2}} + \frac{1}{R_{inj}}\right)}, \qquad (20)$$

$$g_2 = \frac{1}{\omega C_g r_g R_{inj}\left(\frac{1}{r_g} + \frac{1}{R_{d1}} + \frac{1}{R_{d2}} + \frac{1}{R_{inj}}\right)}, \qquad (21)$$

and

$$g_3 = \frac{1}{\omega C_{inj} R_{inj}} \left[1 - \frac{1}{R_{inj}\left(\frac{1}{r_g} + \frac{1}{R_{d1}} + \frac{1}{R_{d2}} + \frac{1}{R_{inj}}\right)}\right]. \qquad (22)$$

Using $\boldsymbol{x}$ and $\boldsymbol{G}$, (16) is expressed as

$$\frac{d\boldsymbol{x}(\theta)}{d\theta} = \boldsymbol{F}\left(\boldsymbol{x}(\theta)\right) + \boldsymbol{G}(\Theta), \qquad (23)$$

which corresponds to (7).

In this paper, numerical waveforms are obtained by solving the differential equations with the forth-order Runge-Kutta method.

C. Free-Running Class-E Oscillator Design

The design specifications for the design example are given as follows: operating frequency $f = 1$ MHz, input voltage $V_{DD} = 12$ V, output quality factor $Q = \omega L_0/R = 5$, output resistance $R = 25$ Ω, RMS voltage across the output resistance $V_o = 9$ V, ratio of the output resonant inductance to the dc-feed inductance $L_0/L_C = 0.1$, $V_{fmax} = 15$ V, $R_{inj} = 2$ kΩ, and $C_{inj} = 0.1$ μF. Because $V_{th} = 3$ V and $V_{DD} = 12$ V, $R_{d1} = 750$ kΩ and $R_{d2} = 250$ kΩ. Additionally, $r_S = 0.16$ Ω, $C_g = 1.78$ nF, and $r_g = 2.17$ Ω were obtained as given in Table I, and all of the ESRs of the inductances are zero in the design process. The class-E free-running oscillator for achieving the class-E ZVS/ZDS conditions can be obtained, as given in Table II, by following design methods previously reported [5], [8]. It should be noted that $v_{inj} = 0$ is given for the free-running oscillator design.

Fig. 4 shows the numerical and experimental waveforms of the free-running class-E oscillator, and Table II gives the measurement results. All experimental element values were measured using a HP4284A LCR meter, and the voltages and cur-

$$\begin{cases} \frac{R}{V_{DD}}\frac{di_C}{d\theta} = \frac{R}{\omega L_C}\left(1 - \frac{v_S}{V_{DD}} - \frac{r_{L_C} i_C}{V_{DD}}\right) \\ \frac{1}{V_{DD}}\frac{dv_S}{d\theta} = \frac{1}{\omega C_S V_{DD}}\left(i_C - \frac{v_S}{R_S} - i\right) \\ \frac{1}{V_{DD}}\frac{dv}{d\theta} = \frac{i}{\omega C_0 V_{DD}} \\ \frac{R}{V_{DD}}\frac{di}{d\theta} = \frac{R}{\omega L_0}\frac{v_S - v - v_1 - v_2 - r_{L_0} i}{V_{DD}} \\ \frac{1}{V_{DD}}\frac{dv_1}{d\theta} = \frac{1}{\omega C_1 V_{DD}}\left(i - \frac{v_1 + v_2}{R}\right) \\ \frac{1}{V_{DD}}\frac{dv_2}{d\theta} = \frac{1}{\omega C_2 V_{DD}}\left(i - \frac{v_1 + v_2}{R} - i_f\right) \\ \frac{r_g}{V_{DD}}\frac{di_f}{d\theta} = \frac{r_g}{\omega L_f}\frac{v_2 - v_f - r_{L_f} i_f}{V_{DD}} \\ \frac{1}{V_{DD}}\frac{dv_g}{d\theta} = \frac{1}{\omega C_g r_g\left(\frac{1}{r_g} + \frac{1}{R_{d1}} + \frac{1}{R_{d2}} + \frac{1}{R_{inj}}\right)}\left\{\frac{i_f}{V_{DD}} + \frac{1}{R_{d1}} + \frac{1}{R_{inj}}\frac{v_{inj} - v_{C_{inj}}}{V_{DD}} - \frac{v_g}{V_{DD}}\left(\frac{1}{R_{d1}} + \frac{1}{R_{d2}} + \frac{1}{R_{inj}}\right)\right\} \\ \frac{1}{V_{DD}}\frac{dv_{C_{inj}}}{d\theta} = \frac{v_{inj} - v_{C_{inj}} - v_f}{\omega C_{inj} R_{inj} V_{DD}} \\ v_f = v_g + \omega C_g r_g \frac{dv_g}{d\theta}. \end{cases} \qquad (16)$$

TABLE II
DESIGN VALUES OF INJECTION-LOCKED CLASS-E OSCILLATOR

	Calculated	Measured	Difference
L_C	199 μH	214 μH	7.5 %
L_0	19.9 μH	19.9 μH	−0.20 %
L_f	16.5 μH	16.5 μH	−0.36 %
C_S	1.50 nF	1.46 nF	−2.5 %
C_0	1.75 nF	1.74 nF	−0.68 %
C_1	1.80 nF	1.79 nF	−0.83 %
C_2	17.3 nF	17.4 nF	−0.38 %
R	25.0 Ω	25.0 Ω	−0.090 %
R_{d1}	750 kΩ	752 kΩ	0.20 %
R_{d2}	250 kΩ	249 kΩ	−0.21 %
r_{L_C}	-	0.0100 Ω	-
r_{L_0}	-	0.503 Ω	-
r_{L_f}	-	0.400 Ω	-
R_{inj}	2 kΩ	1.98 kΩ	−0.80 %
C_{inj}	0.100 μF	0.101 μF	1.4 %
f_{free}	1 MHz	1.0077 MHz	0.77 %
V_{DD}	12.0 V	12.0 V	0.0 %
V_o	9.0 V	8.80 V	−2.2 %
I_c	0.277 A	0.278 A	0.36 %
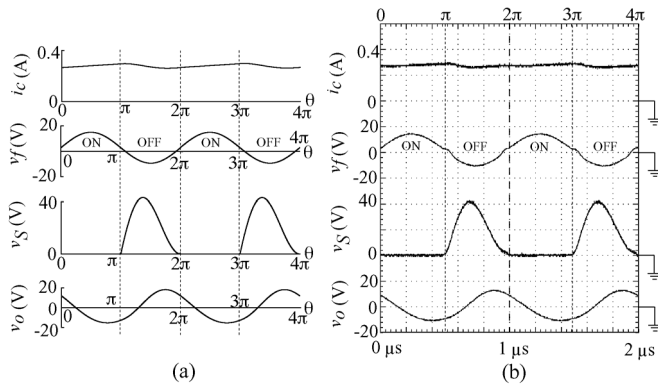
Fig. 4. Waveforms of designed injection-locked class-E oscillator. (a) Numerical waveforms. (b) Experimental waveforms.

rents were measured using a Agilent 3458A multimeter. The parasitic capacitance of the IRF530 MOSFET was estimated to be 270 pF, which was obtained from a previous study [34]. Fig. 4 and Table II show that the experimental results quantitatively agreed with the numerical predictions. In the free-running oscillator, the free-running frequency is 1.0077 MHz, which was measured by the multimeter.

V. DERIVATION OF LOCKING RANGES

In this section, the locking ranges for the injection-locked class-E oscillator are estimated on the basis of PRT.

A. Definition of Impulse Sensitivity Function and Linear Response Region

For deriving the locking ranges, it is necessary to obtain the PSF as stated in Section III because $\Gamma(\psi)$ is obtained by the convolution integral of the PSF and the injection signal. The PSF can be regarded as the impulse response of the phase [18], [20], [21], [23], [28]. In the proposed locking-range derivation method, the PSF is obtained numerically.

It is assumed that the free-running class-E oscillator is in the steady state because the phase in (7) is defined in the steady-state. An impulsive voltage perturbation can be injected at any phase of the one-cycle oscillation. Fig. 5 shows an example of the trajectory when the impulse perturbation is injected at
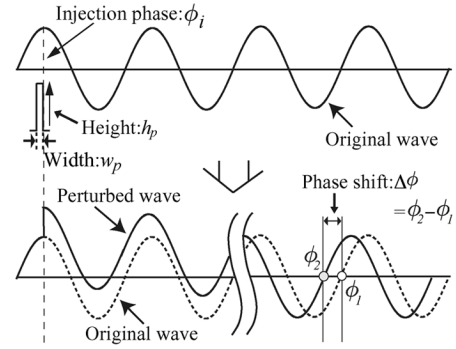
Fig. 5. Phase shift due to impulse perturbation at ϕ_i.
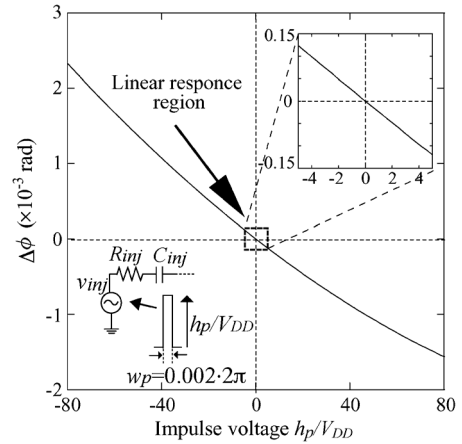
Fig. 6. $\Delta\phi$ of the designed injection-locked class-E oscillator for $\phi_i = 0$.
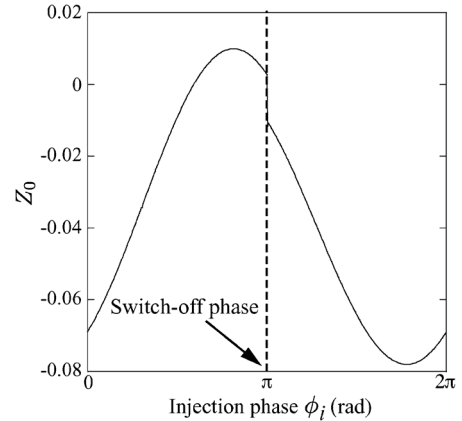
Fig. 7. Impulse sensitivity function (ISF) of the designed injection-locked class-E oscillator.

$\phi = \phi_i$. After injecting the pulse waveform, the waveforms return to the steady state via transient response. However, a phase shift $\Delta\phi$ remains, as shown in Fig. 5. In particular, the phase shift $\Delta\phi$ is expressed as a function of the injection phase ϕ_i. This function is known as the impulse sensitivity function (ISF) [18], [20], [21], [23], [28]. The ISF is apparently equivalent to the PSF because the PSF represents the phase gradient on the limit cycle of the oscillator $\partial\phi/\partial\boldsymbol{x}$. When the ISF is determined numerically, the injection-pulse width w_p and height h_p are important because the phase shift depends on the impulse-perturbation injection phase ϕ_i in addition to the pulse shape. If the pulse is narrow and low, the phase shift is in proportion to the pulse area. The region where $\Delta\phi$ is in proportion to h_p/V_{DD} is defined as the linear response region (LRR). When the ISF is
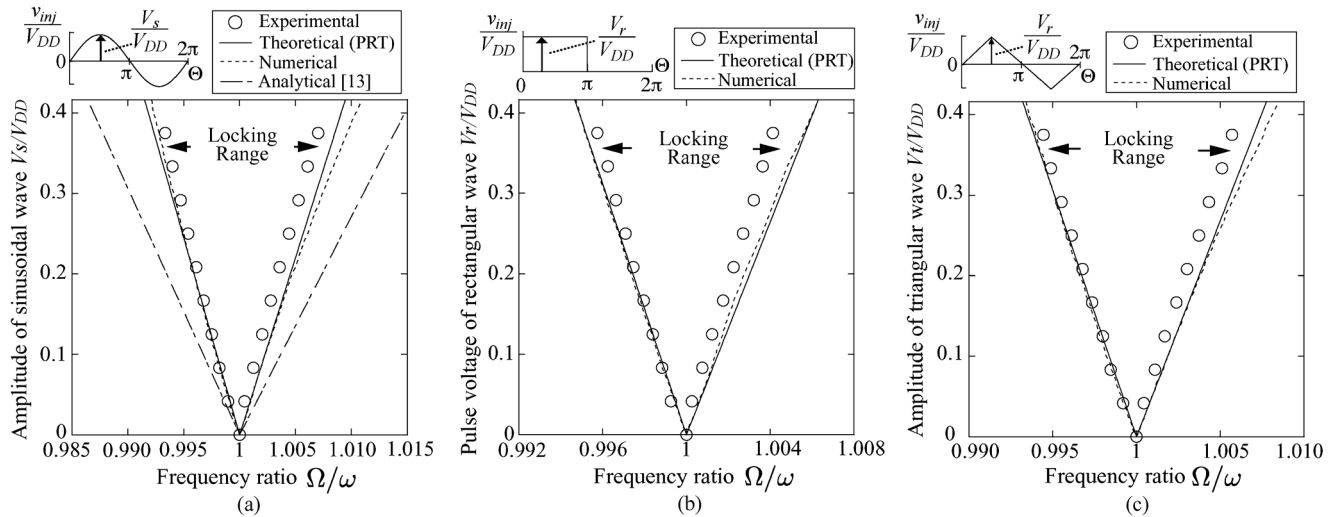
Fig. 8. Experimental, calculated (phase reduction theory; PRT), and numerical locking ranges. (a) Sinusoidal-wave injection. (b) Rectangular-wave injection. (c) Triangular-wave injection.

obtained in this region, it is uniquely determined by normalizing the phase shift by the pulse area.

In this paper, $\Gamma(\psi)$ is obtained from

$$\Gamma(\psi) = \frac{1}{2\pi} \int_0^{2\pi} Z_0(\psi + \Theta) \cdot \frac{v_{inj}(\Theta)}{V_{DD}} d\Theta, \qquad (24)$$

where $Z_0(\phi_i)$ is the ISF.

B. Numerical Derivation of ISF

Fig. 6 shows $\Delta\phi$ as a function of the impulse amplitude for $\phi_i = 0$ and $\omega = 0.002 \cdot 2\pi$. In particular, the injection voltage v_{inj}/V_{DD} is

$$\frac{v_{inj}}{V_{DD}} = \begin{cases} \frac{h_p}{V_{DD}}, & \text{for } \phi_i \leq \theta < w_p \\ 0. & \text{for other} \end{cases} \qquad (25)$$

The pulse-shape waveforms were injected at the instant of switch turn-on ($\phi_i = \theta = 0$), and the phase shifts through the transient state with 5000 periods was plotted. It was confirmed that 5000 periods are sufficiently long for the oscillator to be in the steady state. It is seen from the extended region in Fig. 6 that the phase shift varies linearly with the pulse height. From this figure, the impulse signal that has $h_p/V_{DD} = 0.833$, particularly $h_p = 10$ V, and $w_p = 0.002 \cdot 2\pi$ is used for the ISF derivation.

Fig. 7 shows the ISF of the designed class-E oscillator. The ISF is defined as the phase shift by applying a unit impulse as a function of injection point. It is ensured that the phase shift is in proportion to the pulse area because it is in the LRR, as shown in Fig. 6. Therefore, the ISF is obtained from

$$Z_0(\phi_i) = \frac{\Delta\phi}{\frac{h_p}{V_{DD}} \cdot w_p}. \qquad (26)$$

It is seen in Fig. 7 that a discontinuous point appears at $\phi_i = \pi$, particularly switch turn-off instant, because there was a jump in the switch current at the turn-off instant, as shown in Fig. 2. In contrast, Z_0 at $\phi_i = 2\pi$, particularly turn-on instant, was continuous, as shown in Fig. 7. This is because the class-E ZVS/ZDS conditions, which are given in (1), were achieved. Because of these conditions, both the switch current and voltage waveforms were continuous at $\theta = 2\pi$.
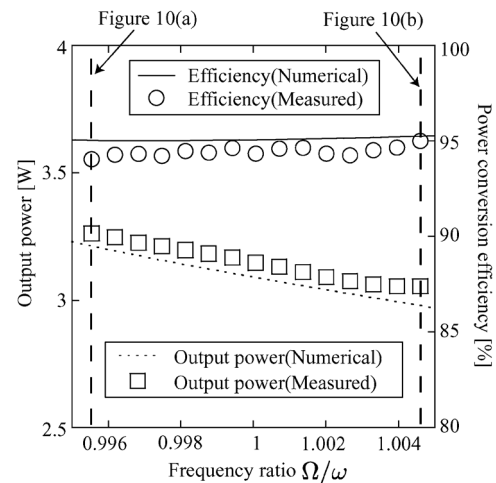
Fig. 9. Experimental and numerical output power and power conversion efficiency in the locking range of the sinusoidal-wave injection at $V_s/V_{DD} = 0.250$.

C. Locking Ranges of Designed Oscillator

In this paper, the locking ranges of the class-E oscillator for three types of injection signals v_{inj}, which are sinusoidal, rectangular, and triangle waveform signals, are predicted. The injection signals are expressed as

1) sinusoidal wave

$$\frac{v_{inj}}{V_{DD}} = \frac{V_s}{V_{DD}} \sin \Theta, \qquad (27)$$

2) rectangular wave

$$\frac{v_{inj}}{V_{DD}} = \begin{cases} \frac{V_r}{V_{DD}}, & \text{for } 0 \leq \Theta < \pi \\ 0, & \text{for } \pi \leq \Theta < 2\pi \end{cases} \qquad (28)$$

and

3) triangle wave

$$\frac{v_{inj}}{V_{DD}} = \begin{cases} \frac{2V_t}{\pi V_{DD}}\Theta, & \text{for } 0 \leq \Theta < \frac{\pi}{2} \\ \frac{V_t}{V_{DD}} - \frac{2V_t}{\pi V_{DD}}\left(\Theta - \frac{\pi}{2}\right), & \text{for } \frac{\pi}{2} \leq \Theta < \frac{3\pi}{2} \\ \frac{-V_t}{V_{DD}} + \frac{2V_t}{\pi V_{DD}}\left(\Theta - \frac{3\pi}{2}\right), & \text{for } \frac{3\pi}{2} \leq \Theta < 2\pi \end{cases} \qquad (29)$$

where V_s, V_r, and V_t are the peak values of each waveforms.
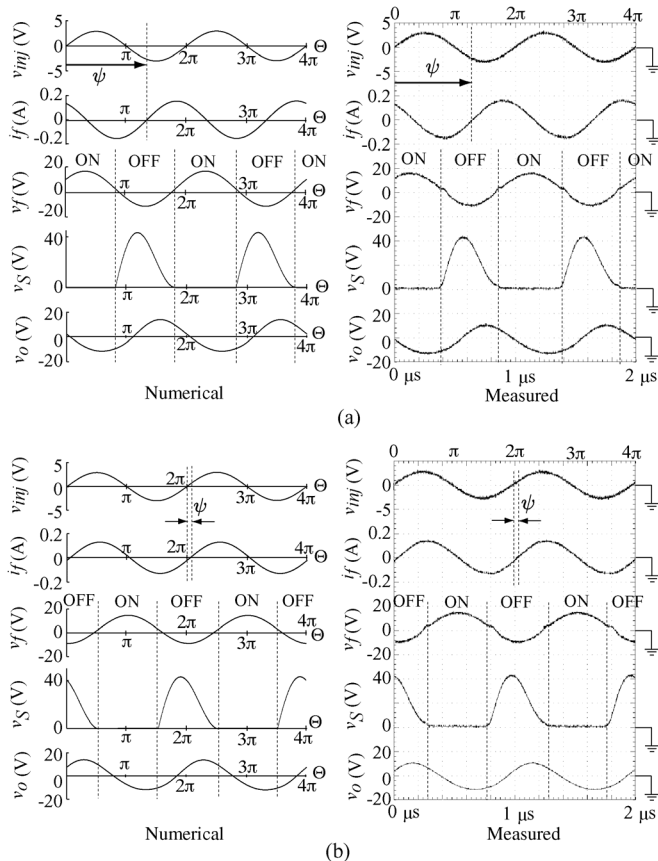
Fig. 10. Waveforms at $V_s = 3$ V for (a) $\Omega = 0.99551\omega$ and (b) $\Omega = 1.00449\omega$.

$\Gamma(\psi)$ can be obtained numerically by the convolution integral of the ISF shown in Fig. 7 and the injection signal. For the numerical calculations, the 50th order Fourier expansion of the ISF is applied to the convolution integral calculations with the injection waveforms, which provides an accurate approximation.

Fig. 8 shows the locking ranges of the designed injection-locked class-E oscillator for each injection waveform. It is shown in (24) that $\Gamma(\psi)$ varies linearly with the injection signal. Therefore, the theoretical locking ranges increase in proportion to the peak voltage of the injection voltages. The numerical results in Fig. 8 were obtained by the calculation algorithm in [14]. It is shown in Fig. 8 that the theoretical locking ranges quantitatively agree with the experimental and the numerical ranges, regardless of injection-signal waveforms, which validates the effectiveness and usefulness of the locking-range predictions based on PRT. Because (15) and (16) are normalized by the free-running frequency, it can be stated that the locking ranges in Fig. 8 are independent of the specified operating frequency.

Fig. 8(a) also shows the analytical locking range from a previous study [13] based on Adler's equation [16]. It can be stated that the proposed locking-range prediction method gives more accurate locking ranges than the values from the analytical method [13]. Compared with the analytical derivation method of locking ranges [13], [32], [33], the numerical derivation method presented in this paper includes the following advantages: 1) When the circuit equations are formulated, the locking ranges can be estimated following the similar calculations steps presented in this paper. In particular, the proposed method can be adapted to any practical oscillators with many variables. In addition, the accurate locking ranges can be obtained by formulating circuit model in detail. 2) Locking ranges on any injection-signal waveform can be efficiently obtained because the ISF is independent of the injection-signal waveform.

Fig. 9 shows the output power and power conversion efficiency as a function of frequency ratio for the sinusoidal-wave injection at $V_s/V_{DD} = 0.25$ ($V_s = 3.0$ V). For obtaining the numerical results in Fig. 9, the ESRs of the inductances given in Table II were considered. In this figure, it is shown that a power conversion efficiency of more than 93% can be kept in all locking ranges. This is because the injection signal does not affect the switch-voltage waveform, and the class-E ZVS/ZDS conditions can be achieved. Fig. 10 shows the numerical and measured waveforms for $\Omega = 0.99551\omega$ and $\Omega = 1.00449\omega$ at $V_s = 3$ V. It is shown in the figure that the class-E ZVS/ZDS conditions were satisfied in both numerical and measured switch-voltage waveforms. The figure also shows that the oscillation frequencies were locked with the injection-signal frequencies in both Fig. 10(a) and (b). Additionally, it was confirmed that the phase shift between v_{inj} and i_f, particularly ψ in Fig. 10(a), is different from that in Fig. 10(b).

VI. CONCLUSION

This paper has presented the numerical derivation method of the locking range for the injection-locked class-E oscillator using PRT. It is possible to obtain the locking ranges on any injection-signal waveform accurately from PRT with low computation cost. The predicted locking ranges from the proposed locking-range derivation method quantitatively agree with those obtained from the simulations and circuit experiments, which shows the validity of this method.

REFERENCES

[1] D. Ahn and S. Hong, "Class-D CMOS oscillators," *IEEE J. Solid-State Circuits*, vol. 48, no. 12, pp. 3105–3119, Dec. 2013.

[2] J. Ebert and M. Kazimierczuk, "Class E high-efficiency tuned power oscillator," *IEEE J. Solid-State Circuits*, vol. SC-16, no. 2, pp. 62–66, Apr. 1981.

[3] D. V. Chernov, M. K. Kazimierczuk, and V. G. Krizhanovski, "Class-E MOSFET low-voltage power oscillator," in *Proc. IEEE ISCAS*, Phoenix, AZ, May 2002, vol. 5, pp. 509–512.

[4] M. K. Kazimierczuk, V. G. Krizhanovski, J. V. Rassokhina, and D. V. Chernov, "Class-E MOSFET tuned power oscillator design procedure," *IEEE Trans. Circuits Syst. I, Reg. Papers*, vol. 52, no. 6, pp. 1138–1147, Jun. 2005.

[5] H. Hase, H. Sekiya, J. Lu, and T. Yahagi, "Novel design procedure for MOSFET class-E oscillator," *IEICE Trans. Fund.*, vol. E87-A, no. 9, pp. 2241–2247, Sep. 2004.

[6] V. G. Krizhanovski, D. V. Chernov, and M. K. Kazimierczuk, "Low-voltage electronic ballast based on class E oscillator," *IEEE Trans. Power Electron.*, vol. 22, no. 3, pp. 863–870, May 2007.

[7] L. R. Nerone, "Novel self-oscillating class E ballast for compact fluorescent lamps," *IEEE Trans. Power Electron.*, vol. 16, no. 2, pp. 175–183, Mar. 2001.

[8] H. Hase, H. Sekiya, J. Lu, and T. Yahagi, "Resonant dc/dc converter with class E oscillator," *IEEE Trans. Circuits Syst. I, Reg. Papers*, vol. 53, no. 9, pp. 2025–2035, Sep. 2006.

[9] T. Andersen, S. K. Christensen, A. Knott, and M. A. E. Andersen, "A VHF class E DC-DC converter with self-oscillating gate driver," in *Proc. IEEE APEC*, Fort Worth, TX, USA, Mar. 2011, pp. 885–891.

[10] C. M. Zierhofer and E. S. Hochmair, "High-efficiency coupling-insensitive transcutaneous power and data transmission via an inductive link," *IEEE Trans. Biomed. Eng.*, vol. 37, no. 7, pp. 716–722, Jul. 1990.

[11] M. Qingyun, M. R. Haider, Y. Song, and S. K. Islam, "Power-oscillator based high efficiency inductive power-link for transcutaneous power transmission," in *Proc. IEEE MWSCAS*, Seattle, WA, USA, Aug. 2010, pp. 537–540.

[12] F. Ellinger, U. Lott, and W. Bachtold, "Design of a low-supply-voltage high-efficiency Class-E voltage-controlled MMIC oscillator at C-band," *IEEE Trans. Microw. Theory Tech.*, vol. 49, no. 1, pp. 203–206, Jan. 2001.

[13] M. K. Kazimierczuk, V. G. Krizhanovski, J. V. Rassokhina, and D. V. Chernov, "Injection-locked class-E oscillator," *IEEE Trans. Circuits Syst. I, Reg. Papers*, vol. 53, no. 6, pp. 1214–1222, Jun. 2006.

[14] T. Nagashima, X. Wei, H. Tanaka, and H. Sekiya, "Numerical derivations of locking ranges for injection-locked class-E oscillator," in *Proc. IEEE PEDS*, Kitakyushu, Japan, Apr. 2013, pp. 1021–1024.

[15] M. Matsuo, H. Sekiya, T. Suetsugu, K. Shinoda, and S. Mori, "Design of a high-efficiency class DE tuned power oscillator," *IEEE Trans. Circuits Syst. I, Fundam. Theory Appl.*, vol. 47, no. 11, pp. 1645–1649, Nov. 2000.

[16] R. A. Adler, "Study of locking phenomena in oscillators," *Proc. IRE*, vol. 34, no. 6, pp. 351–357, Jun. 1946.

[17] A. Mirzaei, M. E. Heidari, R. Bagheri, S. Chehrazi, and A. A. Abidi, "The quadrature LC oscillator: A complete portrait based on injection locking," *IEEE J. Solid-State Circuits*, vol. 42, no. 9, pp. 1916–1932, Sept. 2007.

[18] P. Maffezzoni, "Analysis of oscillator injection locking through phase-domain impulse-response," *IEEE Trans. Circuits Syst. I, Reg. Papers*, vol. 55, no. 5, pp. 1297–1305, Jun. 2008.

[19] C. T. Chen, T. S. Horng, K. C. Peng, and C. J. Li, "High-gain and high-efficiency EER/Polar transmitters using injection-locked oscillators," *IEEE Trans. Microw. Theory Tech.*, vol. 60, no. 12, pp. 4117–4128, Dec. 2012.

[20] D. Dunwell and A. C. Carusone, "Modeling oscillator injection locking using the phase domain response," *IEEE Trans. Circuits Syst. I, Reg. Papers*, vol. 60, no. 11, pp. 2823–2833, Nov. 2013.

[21] P. Maffezzoni, "Nonlinear phase-domain macromodeling of injection-locked frequency dividers," *IEEE Trans. Circuits Syst. I, Reg. Papers*, vol. 60, no. 11, pp. 2878–2887, Nov. 2013.

[22] P. Bhansali and J. Roychowdhury, "Gen-Adler: The generalized Adler's equation for injection locking analysis in oscillators," in *Proc. ASP-DAC*, Yokohama, Japan, Jan. 2009, pp. 522–527.

[23] A. Hajimiri and T. H. Lee, "A general theory of phase noise in electrical oscillators," *IEEE J. Solid-State Circuits*, vol. 33, no. 2, pp. 179–194, Feb. 1998.

[24] Y. Kuramoto, *Chemical Oscillations, Waves, Turbulence*. New York: Springer-Verlag, 1984.

[25] A. T. Winfree, *The Geometry of Biological Time*. New York: Springer, 1980.

[26] A. Pikovsky, M. Rosenblum, and J. Kurths, *Synchronization: A Universal Concept in Nonlinear Sciences*. Cambridge, U.K.: Cambridge Univ. Press, 2001.

[27] S. Boccaletti, J. Kurths, G. Osipov, D. L. Valladares, and C. S. Zhou, "The synchronization of chaotic systems," *Phys. Rep.*, vol. 366, no. 1/2, pp. 1–101, Aug. 2002.

[28] H. Tanaka, A. Hasegawa, H. Mizuno, and T. Endo, "Synchronizability of distributed clock oscillators," *IEEE Trans. Circuits Syst. I, Fundam. Theory Appl.*, vol. 49, no. 9, pp. 1271–1278, Sep. 2002.

[29] M. Bonnin, F. Corinto, and M. Gilli, "A phase model approach synchronization analysis of coupled nonlinear oscillators," in *Proc. ECCTD*, Antalya, Turkey, Aug. 2009, pp. 335–338.

[30] M. Bonnin, F. Corinto, and M. Gilli, "Phase model reduction and synchronization of nonlinear oscillators by a periodic force," in *Proc. ISCAS*, Paris, France, May 2010, pp. 3385–3388.

[31] M. Bonnin and F. Corinto, "Phase noise and noise induced frequency shift in stochastic nonlinear oscillators," *IEEE Trans. Circuits Syst. I, Reg. Papers*, vol. 60, no. 8, pp. 2104–2115, Aug. 2013.

[32] A. Buonomo and A. L. Schiavo, "Analytical approach to the study of injection-locked frequency dividers," *IEEE Trans. Circuits Syst. I, Reg. Papers*, vol. 60, no. 1, pp. 51–62, Jan. 2013.

[33] A. Buonomo, A. L Schiavo, M. A. Awan, M. S. Asghar, and M. P. Kennedy, "A CMOS injection-locked frequency divider optimized for divide-by-two and divide-by-three operation," *IEEE Trans. Circuits Syst. I, Reg. Papers*, vol. 60, no. 12, pp. 3126–3135, Dec. 2013.

[34] T. Suetsugu and M. K. Kazimierczuk, "Comparison of class-E amplifier with nonlinear and linear shunt capacitance," *IEEE Trans. Circuits Syst. I, Fundam. Theory Appl.*, vol. 50, no. 8, pp. 1089–1097, Aug. 2003.

Tomoharu Nagashima (S'11) was born in Saitama, Japan, on February 4, 1989. He received the B.E. and M.E. degrees from Chiba University, Chiba, Japan, in 2011 and 2012, respectively. He is currently working toward the Ph.D. degree at Chiba University.

His current research interest is in resonant dc/dc power converters, dc/ac inverters, and wireless power transfer systems.

Xiuqin Wei (S'10–M'12) was born in Fujian, China, on December 7, 1983. She received the B.E. degree from Fuzhou University, China, in 2005, and the Ph.D. degree from Chiba University, Japan, in 2012.

Since April 2012, she has been with Fukuoka University, Fukuoka, Japan, and she is now an Assistant Professor at the Department of Electronics Engineering and Computer Science. Her research interests include high frequency power amplifiers.

Hisa-Aki Tanaka (S'93–M'95) received the B.E. degree in electrical engineering and the M.E. and D.E. degrees in electronics and communication engineering from Waseda University, Tokyo, Japan, in 1990, 1992, and 1995, respectively.

From 1996 to 1997, he was a visiting researcher with EECS Department, UC Berkeley. From 1997 to 2001, he was with the Sony Computer Science Laboratory. In 2001, he joined the Department of Electronic Engineering, Faculty of Electro-Communications, University of Electro-Communications, Tokyo, Japan, as an Associate Professor. His current research interests are in synchronization issues in computing and communication systems as well as nonlinear physics.

Dr. Tanaka received the 1995–1997 Research Fellowships of the Japan Society for the Promotion for Young Scientists. He is the holder of twelve patents. He was the recipient of the 2007, 2008, and the 2010 Best Paper Award respectively from the Telecommunications Advancement Foundation.

Hiroo Sekiya (S'97–M'01–SM'11) was born in Tokyo, Japan, on July 5, 1973. He received the B.E., M.E., and Ph.D. degrees in electrical engineering from Keio University, Yokohama, Japan, in 1996, 1998, and 2001, respectively.

Since April 2001, he has been with Chiba University, Chiba, Japan, and now he is an Associate Professor at Graduate School of Advanced Integration Science. From February 2008 to February 2010, he was with the Department of Electrical Engineering, Wright State University, Dayton, OH, USA as a Visiting Scholar. His research interests include high-frequency high-efficiency tuned power amplifiers, resonant dc/dc power converters, dc/ac inverters, and digital signal processing for wireless communications.

Dr. Sekiya is a member of the Institute of Electronics, Information, and Communication Engineers (IEICE) of Japan, the Information Processing Society of Japan (IPSJ), and the Research Institute of Signal Processing (RISP), Japan.